2011-12-08

Characterization of a micromachined vertically deformable varying-pitch grating for a spectrometer

Kim, B.; Phamduy, P.; Sinibaldi, J.; Karunasiri, G.

IOP Publishing

Kim, B., et al. "Characterization of a micromachined vertically deformable varying-pitch grating for a spectrometer." Journal of Micromechanics and Microengineering 22.1 (2011): 015001.
http://hdl.handle.net/10945/60723

J. Micromech. Microeng. **22** (2012) 015001 (11pp) doi:10.1088/0960-1317/22/1/015001

Characterization of a micromachined vertically deformable varying-pitch grating for a spectrometer

B Kim[1,2,4], P Phamduy[1], J Sinibaldi[3] and G Karunasiri[3]

[1] Department of Mechanical Engineering, University of Massachusetts, Lowell, MA 01854, USA
[2] NSF Center for High-Rate Nanomanufacturing, University of Massachusetts, Lowell, MA 01854, USA
[3] Department of Physics, Naval Postgraduate School, Monterey, CA 93943, USA

E-mail: byungki_kim@uml.edu

Received 15 June 2011, in final form 12 October 2011
Published 8 December 2011
Online at stacks.iop.org/JMM/22/015001

Abstract
A new type of micromachined vertically deformable varying-pitch grating is designed and fabricated. Its characterization and its feasibility as a spectrometer are presented. The deformable grating shows a 0.7 μm working range and 3.6 kHz bandwidth. Its characterization and its feasibility as a spectrometer are presented. The varying-pitch grating has the ability to detect an individual wavelength with a single detector by physical scanning. Its deformable capability can increase intensity and resolution at a specific wavelength. Those two capabilities are experimentally demonstrated.

(Some figures in this article are in colour only in the electronic version)

1. Introduction

A grating is an optical component that enables the dispersion of incident light into angular directions corresponding to the properties of the grating for a given wavelength of the incident light. This characteristic of gratings has been used in scanners, optical switches, displays, and spectrometers. MEMS or micromachined gratings have demonstrated advantages over conventional ones. Modulation of a deformable grating, called the silicon light valve, which was originally demonstrated by Solgaard *et al* [1], opens up its application for optical switch and display. After this, numerous MEMS gratings are presented to steer light. For example, Zhou *et al* [2] present a grating offering a dynamic operation to steer incident lights in device level while minimizing degradation of optical performance. MEMS variable blaze gratings (VBGs) are also developed to increase diffraction efficiency by adjusting blaze angle to direct the majority of the diffracted light into a specific direction [3, 4].

Such an advancement of the MEMS grating led to the development of visible and near-infrared MEMS spectrometers, capable of determining the presence of certain molecules in a testing sample. Grating-based spectrometers [5–8], a standing-wave transform spectrometer [9], and a tunable filter-based spectrometer [10] have been successfully fabricated using micromachining techniques. There are two notable spectrometers using a MEMS grating. The polychromator developed by Hocker *et al* [6] is attractive due to its use of a single photodetector and programmable capability. The traditional grating spectroscopy without mechanical scanning requires an array of detectors. The polychromator requires individual actuation of a large array of mechanical beams or ribbons. The polychromator is used as an optical switch to allow only a specific wavelength to reach the single detector. Thus, the resolution of the spectroscopy is mainly determined by its additional static grating. Manzardo *et al* [8] demonstrate time-scanning Fourier-transform spectroscopy showing a 1.6–5.5 nm resolution in a 400–800 nm wavelength using a lamellar grating which enables a 145 μm optical phase difference. Its drawbacks are that its maximum mechanical displacement is limited by its comb structure and the limited height of the grating limits its practical maximum wavelength for detection.

In this paper, characterization of a new micromachined vertically deformable varying-pitch grating for a spectrometer is presented. It requires a single detector and has the capability

[4] Author to whom any correspondence should be addressed.

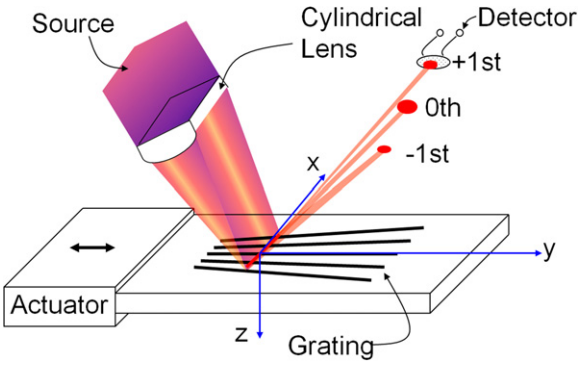

Figure 1. Schematic of the MEMS spectrometer.

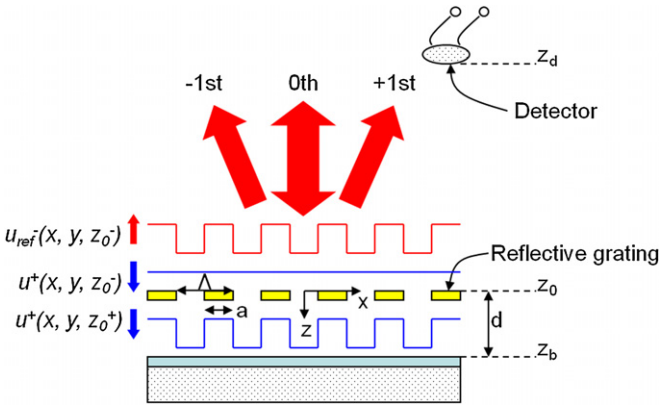

Figure 2. Coordinate system at a certain cross section of y.

to maintain the highest response at the first diffraction order by actuating the grating. The proposed vertically deformable grating is designed to increase optical intensity and spectroscopic resolution at each wavelength although its resolution is low. The varying-pitch grating requires only a single detector while scanning using an actuator. Having those two capabilities in the grating is novel to the authors' knowledge. The strength of the proposed method is that both the source and detector are fixed, while the grating deforms and is translated by the actuator on its side. This paper is focused on the characterization of the vertically deformable varying-pitch grating. After presenting its working principle and characteristics, an experimental result using a narrow band source will demonstrate a proof of concept of the grating having the two capabilities.

2. Working principle

Figure 1 shows a schematic of the spectrometer system where a step grating is used to direct the majority of the light intensity into the first diffraction order. The source light is focused on the grating lines using a cylindrical lens. To scan the light, the grating is translated using an actuator while keeping the lens and the detector fixed. The grating diffracts various wavelengths of the incident source light and the first-order diffraction angle, φ, corresponding to wavelength, λ, is determined by

$$\sin\varphi = \frac{\lambda}{\Lambda}, \tag{1}$$

where Λ is the period of the grating. The period of the grating is varying since the grating is fanned out. To collect the spectral information using a detector fixed at a location given by the first-order diffraction angle, the period of the grating needs to be selected according to $\Lambda = \lambda/\sin\varphi$. Thus, by translating the grating while scanning, different wavelengths can be selected at the fixed location of the detector.

The diffraction pattern from a certain period of the grating is simulated using Fresnel approximation [11]. A coordinate system is defined in figures 1 and 2. The analysis begins at the face of the cylindrical lens where the light source enters orthogonally. The source light, $u^+(x, y, z_{cl}^-)$, just before the cylindrical lens is assumed as a summation of multiple continuous plane waves with n different wavelengths (λ_1–λ_n) or wave numbers (k_1–k_n) in free space. After the source passes the cylindrical lens, it is focused into the grating. The thickness of the diffraction grating is assumed to be zero. The focused light at z_0, $u^+(x, y, z_0^-)$, is assumed to perpendicularly incident on the grating as shown in figure 2. Then, a rectangle function by the grating modifies the field amplitude. After dropping the time dependence, the fields are

$$\begin{aligned} u^+(x, y, z_{cl}^-) &= \sum_{i=1}^{i=n} A_i\, e^{jk_i z_{cl}^-}, \\ u^+(x, y, z_0^-) &= u^+(x, y, z_{cl}^-) P(x, y)\, e^{j\frac{ky^2}{2f}}, \end{aligned} \tag{2}$$

where u^+ means that the light travels in the $+z$ direction. z_0^- and z_0^+ represent the locations just before and after z_0 ($z_0 = 0$). A_i is the amplitude of the ith plane wave. k_i is the wave number given by $2\pi/\lambda_i$. $P(x, y)$ is a pupil function of the cylindrical lens and f is the focal length of the lens. The lens is assumed to be a cylindrical plano-convex lens and the phase by the lens is approximated [12].

The fields after the grating at z_0 and just before the bottom layer at z_b are

$$\begin{aligned} u^+(x, y, z_0^+) &= u^+(x, y, z_0^-) \sum_{m=-l}^{m=l} \mathrm{rect}\left(\frac{x - \Lambda m}{a}\right), \\ u^+(x, y, z_b^-) &= u^+(x, y, z_0^+)\, e^{jk|z_b - z_0|} = u^+(x, y, z_0^+)\, e^{jkd}, \end{aligned} \tag{3}$$

where $\sum$rect is a summation of rectangle functions representing the inverse of the grating and l is the half number of grating fingers. a is the width of the grating fingers. d is the height difference of the top grating and the bottom layer. The light after the grating, $u^+(x, y, z_0^+)$, travels to the bottom layer. Since d is kept to less than a few wavelengths, the light at the bottom layer, $u^+(x, y, z_b^-)$, is assumed to be the same as $u^+(x, y, z_0^+)$ with different phase due to the travel. Part of the source light after the lens, $u^+(x, y, z_0^-)$, reflects back from the top side of the grating. Let this reflected light be $u^-{}_{ref}(x, y, z_0^-)$, then

$$\begin{aligned} &u_{ref}^-(x, y, z_0^-) \\ &= u^+(x, y, z_0^-) R_{top} \left[\mathrm{rect}\left(\frac{x}{2\Lambda l}\right) - \sum_{m=l}^{m=l} \mathrm{rect}\left(\frac{x - \Lambda m}{a}\right)\right], \end{aligned} \tag{4}$$

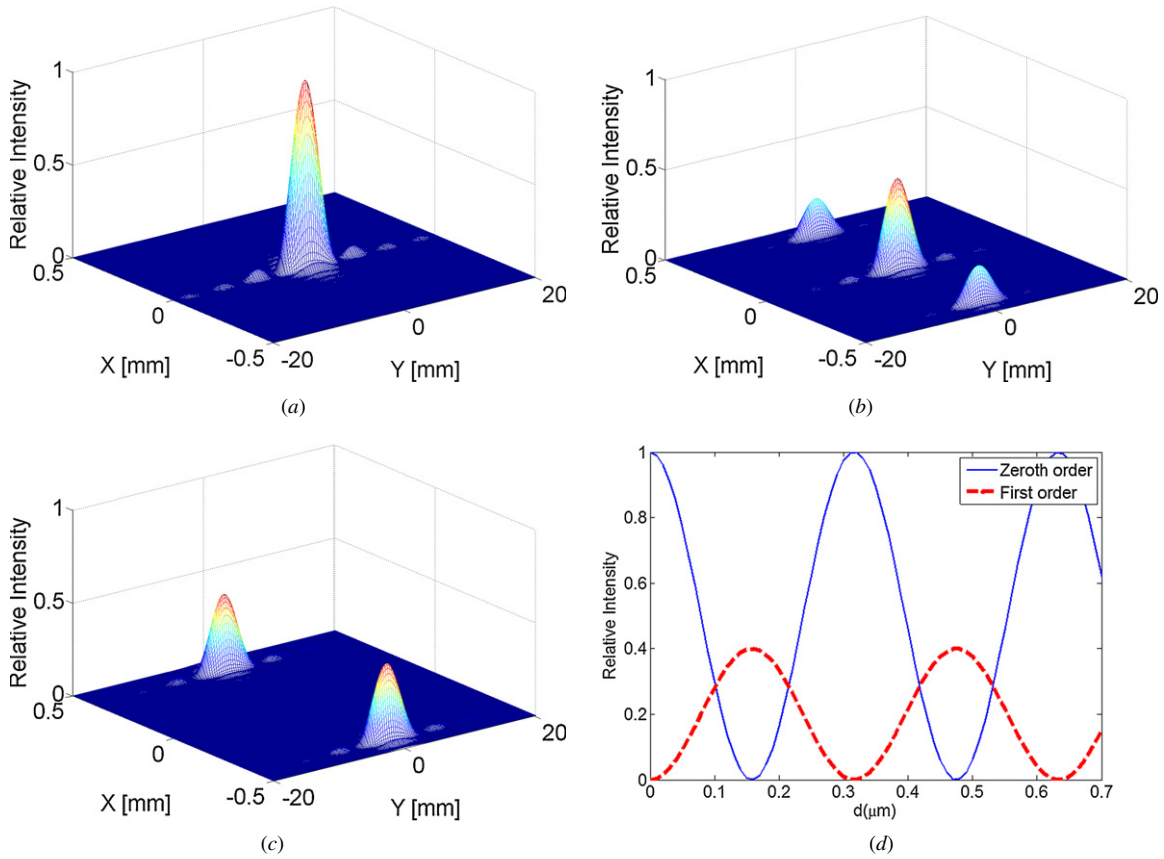

Figure 3. Diffracted intensity at the detector plane for three different d: (*a*) 0 or $\lambda/2$, (*b*) $\lambda/8$, and (*c*) $\lambda/4$. (*d*) Intensity versus d, grating height at zero and first orders.

where R_{top} is a reflection coefficient of the top grating. The subtraction of the rectangular functions in the bracket represents the grating. The light reaching the bottom layer, $u^{+}(x,\ y,\ z_b^{-})$, reflects from the bottom layer and returns to the z_0. Then, the returning field on the grating plane at z_0, $u^{-}(x, y, z_0^{-})$, is the summation of the wave fronts from the top grating and bottom layer which can be written as

$$u^{-}(x, y, z_0^{-}) = u_{\text{ref}}^{-}(x, y, z_0^{-}) + u^{+}(x, y, z_b^{-})R_{\text{bot}}\,\mathrm{e}^{\mathrm{j}kd}$$
$$= u^{+}(x, y, z_0^{-})R_{\text{top}}\left[\text{rect}\left(\frac{x}{2\Lambda l}\right) - \sum_{m=l}^{m=l}\text{rect}\left(\frac{x-\Lambda m}{a}\right)\right]$$
$$+ u^{+}(x, y, z_0^{-})R_{\text{bot}}\,\mathrm{e}^{\mathrm{j}k2d}\sum_{m=-l}^{m=l}\text{rect}\left(\frac{x-\Lambda m}{a}\right), \qquad (5)$$

where R_{bot} is the reflection coefficient at the bottom layer. By Fresnel approximation, the field diffracted from the grating and reaching the detector plane, z_D, is

$$u^{-}(x_1, y_1, z_D) = \frac{\exp(\mathrm{j}kz_D)}{\mathrm{j}\lambda z_D}\exp\left[\mathrm{j}\frac{k}{2z_D}\left(x_1^2 + y_1^2\right)\right]$$
$$\times\int\!\!\int_{-\infty}^{\infty} u\,(x, y)\exp\left[\mathrm{j}\frac{2\pi}{\lambda z_D}\left(x_1 x + y_1 y\right)\right]\mathrm{d}x\mathrm{d}y, \qquad (6)$$

where

$$u\,(x, y) = \left\{u^{-}(x, y, z_0^{-})\exp\left[\mathrm{j}\frac{k}{2z_D}(x^2 + y^2)\right]\right\}.$$

Table 1. Parameters used in the analysis.

λ: wavelength (μm)	0.633
$P(x, y)$: pupil function (inch^2)	1
Λ: period of grating (μm)	36
l: half number of the grating beams	3
a: width of the grating (μm)	18
d: grating height (μm)	0–0.7
R_{top}, R_{bot}: reflection coefficients	1
f: focal length of the cylindrical lens (mm)	100
z_D: the detector plane (mm)	−23

The analysis is done for a source with one wavelength hitting a single grating period. Table 1 summarizes the parameters used in the analysis.

Figures 3(*a*)–(*c*) show the simulated spatial intensity of the diffracted monochromatic source from the grating for three different step heights, d. The intensity at first order is highest when the path difference between the reflected light beams from the step is $\lambda/4$. Kim *et al* [13, 14] reported that the intensity at first order is highest when the grating height d is an odd multiple of a $\lambda/4$ at different application. The simulation demonstrates that the intensity at first order is maximized and zero order is minimized at d of $\lambda/4$, 0.158 μm, or an odd multiple of $\lambda/4$. The pattern along the x-axis is the zero and $\pm$first diffraction orders at different d and the pattern along the y-axis is determined by the cylindrical lens used to make the light focus on the grating and disperse

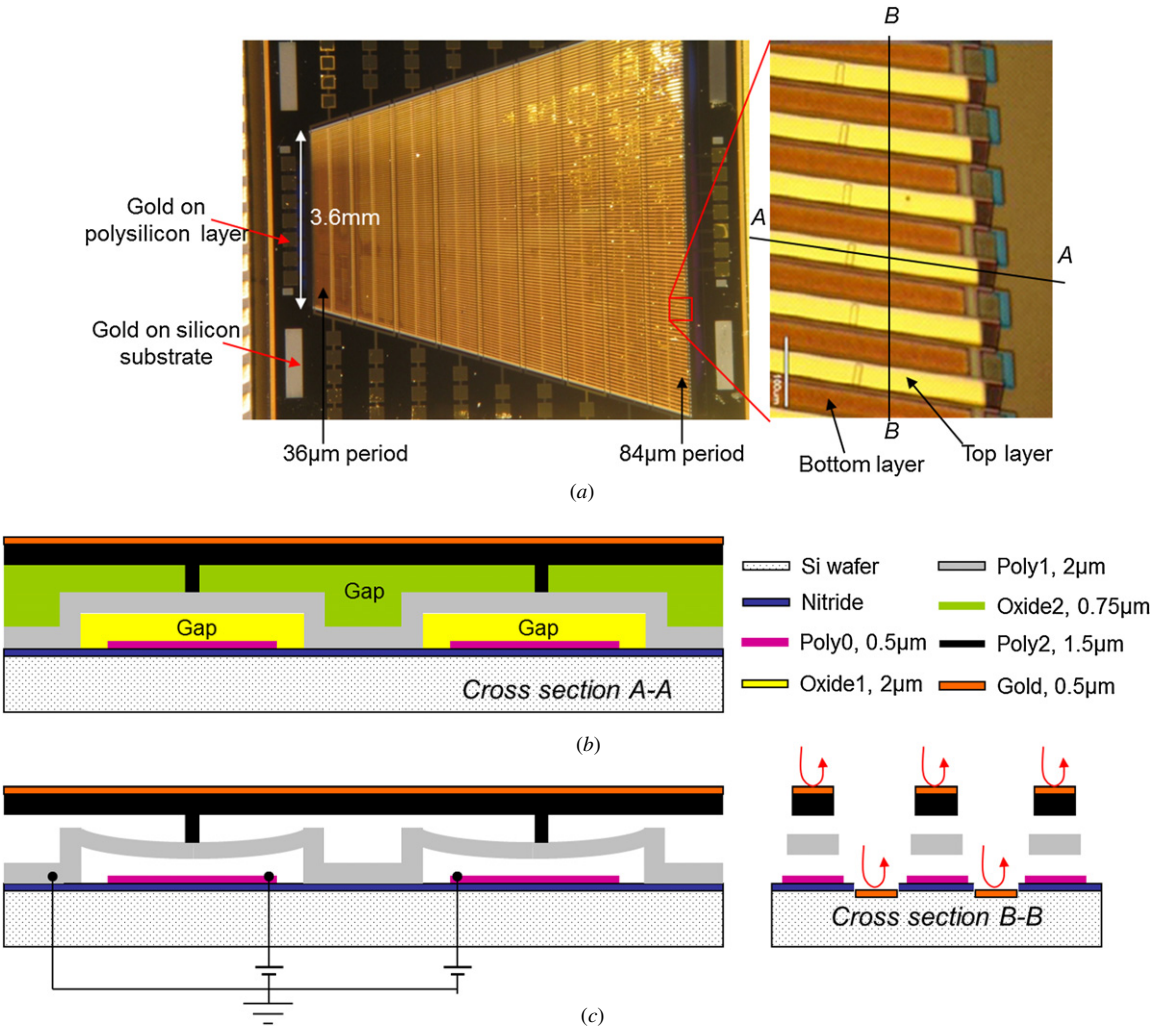

Figure 4. (*a*) Fabricated grating showing the varying periodicity, (*b*) schematic of the cross-sectional view A–A showing the grating structure with layers, (*c*) the grating structure actuated by a voltage bias (left) and schematic of the cross-sectional view B–B (right).

after hitting the grating. The pattern along the *y*-axis is a sinc function by the lens. Figure 3(*d*) shows the intensity change of the zero and first orders at different *d*, the grating height. This demonstrates a need to change the grating height to detect the wavelength at its maximum signal. Since the incident light beam is focused by the cylindrical lens, the diffracted beam diverges as it moves away from the grating and a second cylindrical lens is needed to focus the outgoing beam.

3. Fabrication of the gratings

The grating shown in figure 4(*a*) is fabricated by PolyMUMPs (Multi-User MEMS Processes) run by MEMSCAP [15]. Figures 4(*b*) and (*c*) show a schematic of the grating cross-sectional view before and after release of the grating beam. Figure 4(*a*) also shows the cross-sectional directions, A–A and B–B. In PolyMUMPs, two layers of doped polysilicon are used to make the grating mechanical structure with adjustable step height and two oxide layers serve as sacrificial layers. A gold layer is deposited on the top polysilicon and bottom silicon substrate to enhance the light reflection. But, it turns out that gold barely covers the silicon substrate. Thus, the bottom layer is not as reflective as the top layer. More discussion on this is in the next section. The PolyMUMPs start with a heavily doped silicon wafer. Then, low stress nitride and polysilicon (poly0) layers are deposited. The poly0 layer serves as a bottom electrode as shown in figure 4(*c*). The bottom electrode is patterned by lithography and reactive ion etching (RIE). The first oxide layer (oxide1) is deposited by low-temperature chemical vapor deposition (CVD). The oxide layer is patterned by RIE to protect the bottom electrode and to determine a gap for actuation. The second polysilicon layer (poly1) is deposited by low-pressure CVD. The wafer is annealed at a high temperature after depositing a thin phosphor silicate glass layer to dope the poly1. The poly1 is patterned by RIE to determine the first mechanical structure. The RIE stops on the first oxide (oxide1). The second oxide layer (oxide2) is deposited by low-temperature CVD. The oxide2 is then patterned, and it is etched through RIE to open a space to connect poly1 and the third polysilicon layer (poly2). The poly2 is deposited by the same procedure used for the poly1. After poly2 is patterned to be grating beams, a gold layer is deposited and patterned by a lift-off process. All oxide layers are removed by concentrated HF and the structures are

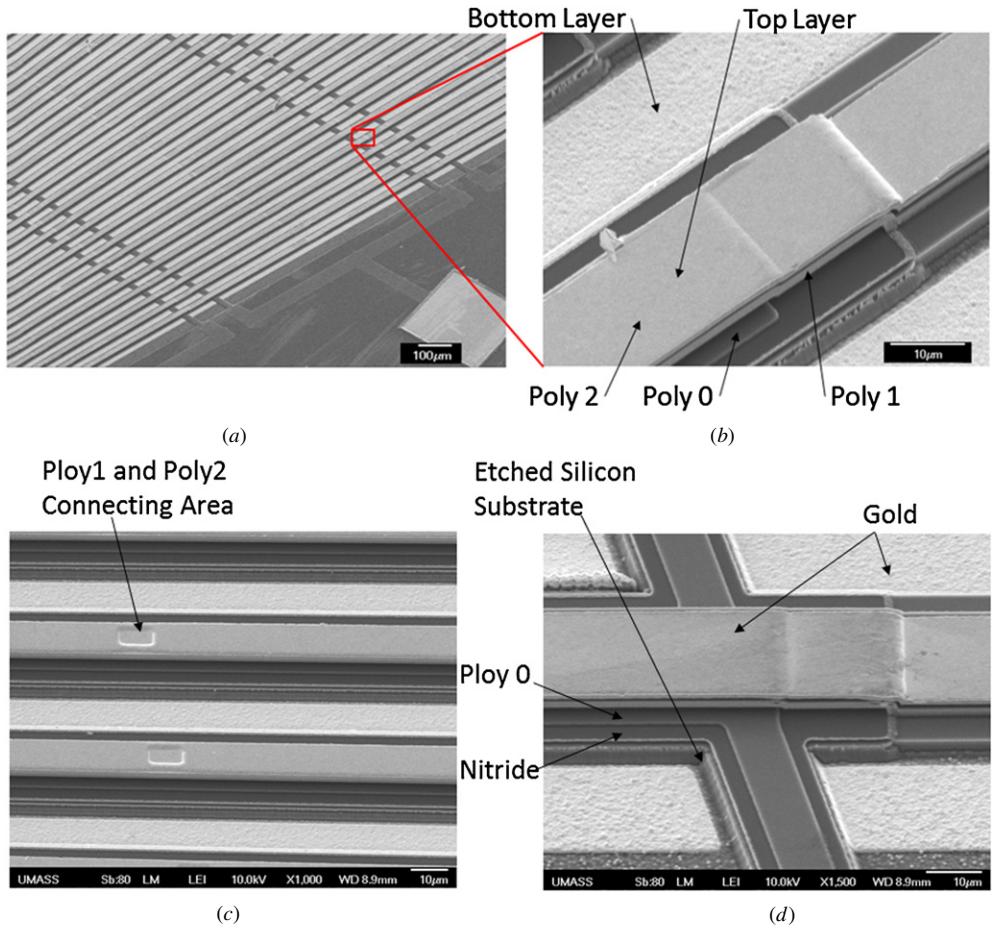

Figure 5. SEM images of (*a*) grating and solder pad, (*b*) top and bottom layer of grating, (*c*) poly1 and poly2 connecting area, and (*d*) etched silicon substrate.

released by a critical point dryer to avoid stiction. The bottom layer between the grating beams is initially covered only with nitride. However, the nitride layer and underneath silicon substrate are etched as shown in figure 5(*d*) by the series of RIE processes to remove the three polysilicon layers and the oxide layers at other locations. Thus, the grating height is further increased from the height measured from the nitride layer. Also, the RIE processes leave a rough surface on the bottom silicon substrate as seen in figure 5(*b*), which is typical after multiple RIE processes.

Such MUMPs are also used in development of the MEMS VBGs [2]. The key structure of the grating is its double bridge between the poly1 and poly2 layers. This design enables the top polysilicon layer to maintain its flatness while the grating is actuated. The design is originally demonstrated in a deformable mirror [16] and a programmable polychromator [6]. After removing the oxide sacrificial layers, the polysilicon double bridge structure can be actuated within the air gap. By applying a dc bias at the poly1 layer and the bottom poly0 electrode as seen in figure 4(*c*), it is viable to control the phase difference of two wavefronts from the top gold layer and bottom layer.

Between the grating fingers, there is a gap revealing the bottom layer which has the same width as the grating beams as seen in figure 4. Each beam has 18 suspended segments of 400 μm span each, with a 360 μm wide electrode underneath. The fabricated grating is composed of 101 mechanical beams whose width is linearly increased from 10 to 34 μm by fanning out the beams. The period of the grating is linearly varied from 36 to 84 μm. The 36 μm period of the grating is designed to diffract short wavelengths and the 84 μm period of the grating is for longer wavelengths. For example, diffraction of the 0.633 μm wavelength from the 36 μm period and the 1.477 μm wavelength from the 84 μm period gives identical diffraction angles of 1°. Thus, by keeping the detector oriented at 1° and translating the grating, the spectral information for wavelengths from 0.633 to 1.477 μm can be probed.

Scanning electron microscopy (JEOL JSM-7401F FE-SEM) provides a clearer side view of the grating structures as shown in figure 5. In figure 5(*a*), poly0 lines are connected to a square solder pad and are embedded under the grating structures. These solder pads are connected to a voltage source. Close-up SEM images of the poly0, poly1 and poly2 layers as shown in figure 5(*b*) confirm the grating schematic, as seen in figure 4(*b*). In figure 5(*c*), poly2 is connected to poly1 through a rectangular hole. Close-up images of the bottom layer as shown in figure 5(*d*) show the etched silicon substrate.

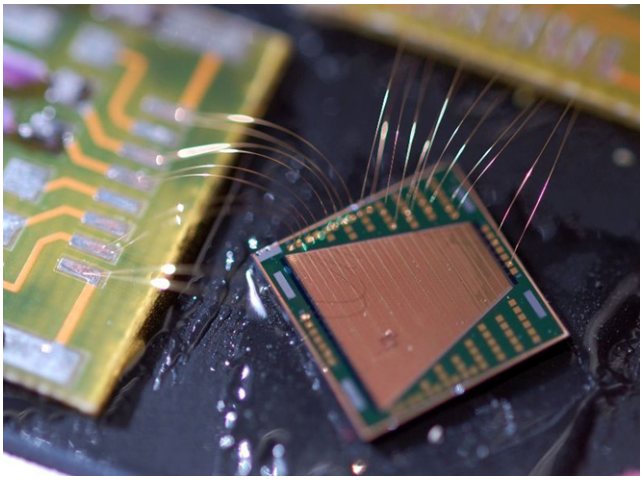

(*a*)

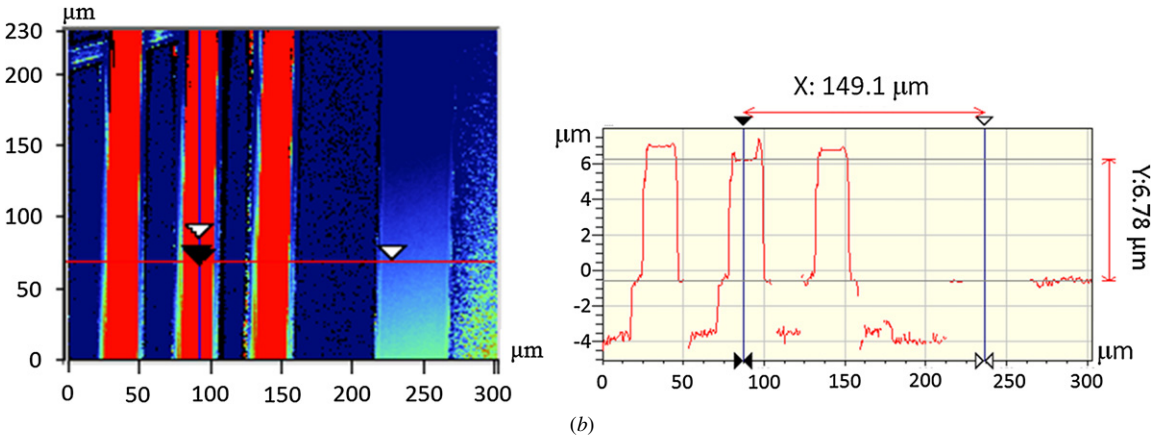

(*b*)

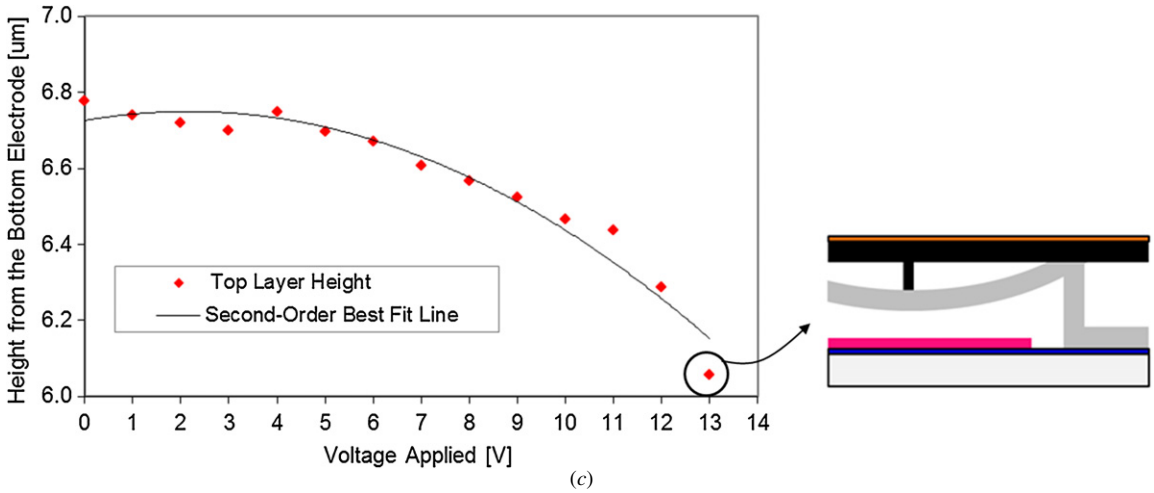

(*c*)

Figure 6. (*a*) Grating after wire bonding, (*b*) optical profilometry measurement for single location with 0 V applied, and (*c*) grating structure height response for applied voltages from optical profilometry measurements. A schematic of collapse of the poly2 layer onto poly1 is shown at 13 V.

4. Experimental results

From experimental observation, when the grating structure is actuated with an applied voltage, there is a change in the height of the top layer. Optical profilometry (Wyko model NT-2000 with 20× lens) measurements characterized the grating displacement for an applied voltage source and determined the maximum voltage the structure can withstand. The height of a poly2 bridge is examined from optical profilometry measurements made of the grating, while a voltage source connected to the grating increases in increments of 1 V. The grating is connected to a voltage source by gold wire bonding as depicted in figure 6(*a*). Figure 6(*b*) shows an optical profilometry measurement of a consistent location on the beam

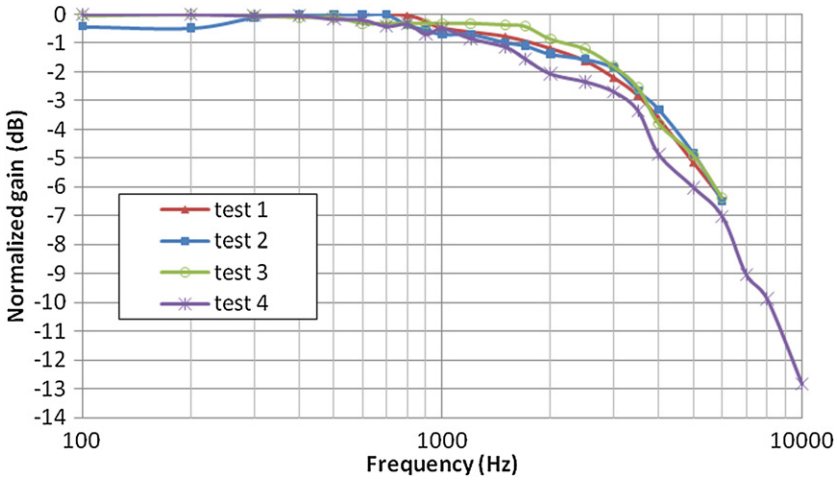

Figure 7. Frequency response of the grating.

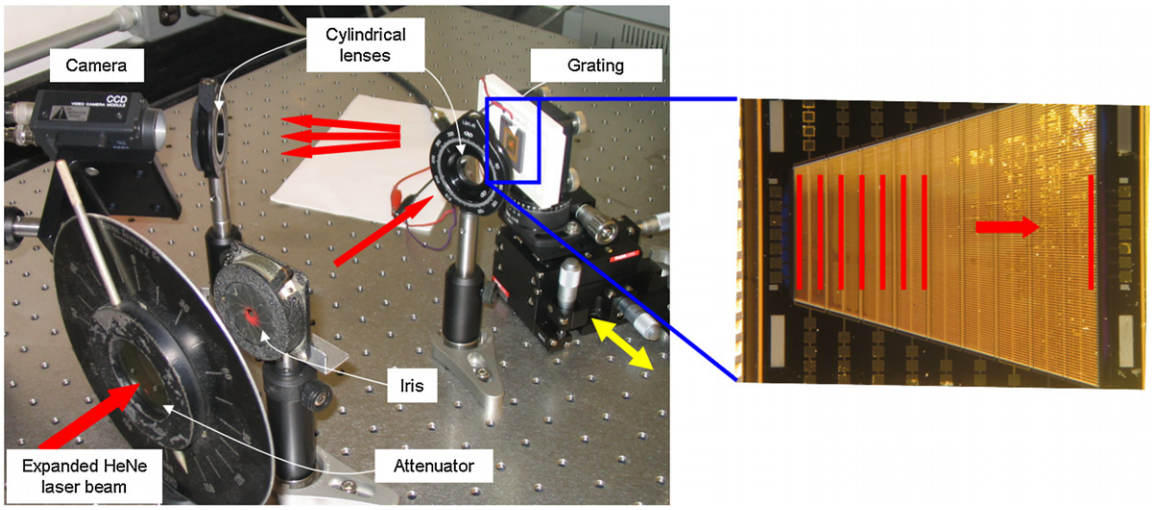

Figure 8. A photo of the experiment setup.

when no voltage is applied to the grating. The right image in figure 6(*b*) shows the grating height as 6.78 μm from the bottom electrode (poly0), which is very close to 6.75 μm, the summation of thicknesses of the subsequent layers from oxide1 to gold. For this measurement, the bottom electrode is chosen as a reference plane due to its good surface quality. The grating height from the bottom silicon substrate between the grating beams is estimated to be 9.96 μm. The additional 3.19 μm comes from poly0, the nitride layer, and the etched silicon substrate as discussed in the previous section. By increasing the applied voltage, as seen in figure 6(*c*), the grating height decreases. The grating drops 0.7 μm from its initial height at 13 V where the poly1 and poly2 layers may be in contact as seen in figure 6(*c*) or very close to contact considering the oxide2 thickness of 0.75 μm.

The grating has a working frequency range limit up to 3.60 kHz that is determined experimentally from its frequency response, as seen in figure 7. The tests in figure 7 correspond to the same experiment run at four different times and different locations on the same grating to show that the cutoff frequency is relatively the same across the grating. The grating is actuated with an ac signal, powered by a function generator. A HeNe laser beam is then concentrated on a bridge on the grating and reflected into a photo detector. The output voltage from the detector and the input ac voltage are used to determine the gain of the frequency response. The average cutoff frequency for the tests is 3.60 kHz with a standard deviation of 240 Hz.

The fabricated spectrometer is characterized using the setup schematically shown in figure 1 and its physical setup shown in figure 8 using a HeNe laser (Research Electro Optics, model# LHRP-0201) as the light source. To achieve sharp peaks at the zero and first diffracted orders, the HeNe laser is intentionally expanded and the width of the focused line is controlled by an iris. The focusing of the HeNe laser beam on the grating is performed with the aid of a cylindrical lens. The diffracted beam is condensed by a second identical cylindrical lens and imaged using a CCD camera (Sony CCD monochrome, XC-75, 765 $\times$ 494 pixels, 8.4 $\times$ 9.8 mm^2/pixel). The distance from the grating to the CCD camera is 23.4 cm and incident angle of the beam into the grating is 22.5°. A manual actuator is used to scan the focused laser beam on the grating with periods from 36 to 84 μm.

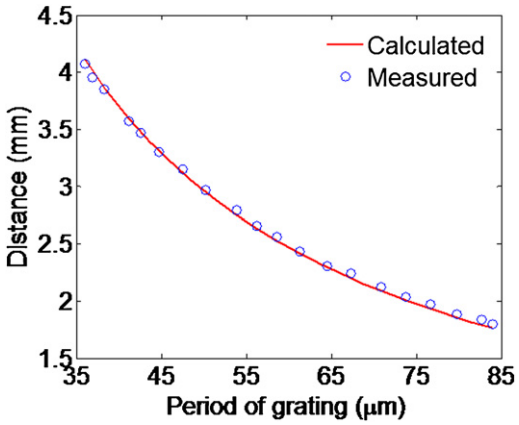

Figure 9. Period of the grating versus distance between the zero and first diffraction orders.

Figure 9 demonstrates the location of the first diffraction order defined by equation (1). The theoretical distance in the figure is calculated by the distance from the grating to the camera times $\tan\varphi = 23.4\ \text{cm} \times \tan[\sin^{-1}(\lambda/\Lambda)]$. The measured data are well matched with these calculated ones.

Figure 10(*a*) shows the measured intensity of the diffracted beam from the 36 to 84 μm periods to determine the spectral resolution of the grating. It appears that there is a fabrication problem in the grating between 3.5 and 4 mm used in this experiment. The peaks at that range are not as sharp as others in the range. Thus, the first orders in that range are not included. The reason the intensities at the first order vary could be that the surface quality of the grating beam and the bottom layer is not uniform at each grating period. This can explain the varying intensity at each location of measurement. Using the Rayleigh criterion of resolution [11], the minimum resolvable wavelengths are estimated to be 17 and 73 nm from 36 to 84 μm grating periodicities, respectively. Images (8-bit gray scale) with the zero and first orders are recorded on the CCD while the grating is scanned by a HeNe laser. Then, the zero order at each grating period is overlapped and the first order is displayed as shown in figure 10(*a*). The intensity of the zero and first orders in the *y*-axis is obtained from each image datum (each pixel value up to 256). From figure 10(*a*), the resolution is estimated by applying the Rayleigh criterion. The resolution at each period of grating is shown in figure 10(*b*) for the two different gratings. The resolution is determined by the assumption that from each period of grating a 0.633 μm wavelength is measured and after that wavelength of up to 1.477 μm is measured. Then, the total wavelength range will be 0.844 μm. The scanning distance from peak to adjacent peak shown in figure 10(*a*) is equivalent to a detectable resolution out of the whole range. For example, the resolution of 17 nm at a 38.5 μm period of grating 1 shown in figure 10(*b*) comes from the scanning of 0.096 μm from 38.453 μm grating period to 38.549 μm grating period. 0.096 μm is equivalent to the 17 nm resolution for the total wavelength range by calculation of 0.096/(84–36)∗0.844. The resolution of 68.6 nm at 82.8 μm shown in figure 10(*b*) comes from a 0.39 μm grating period

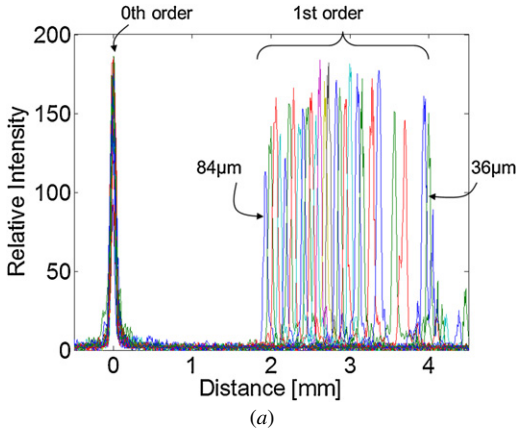

(*a*)

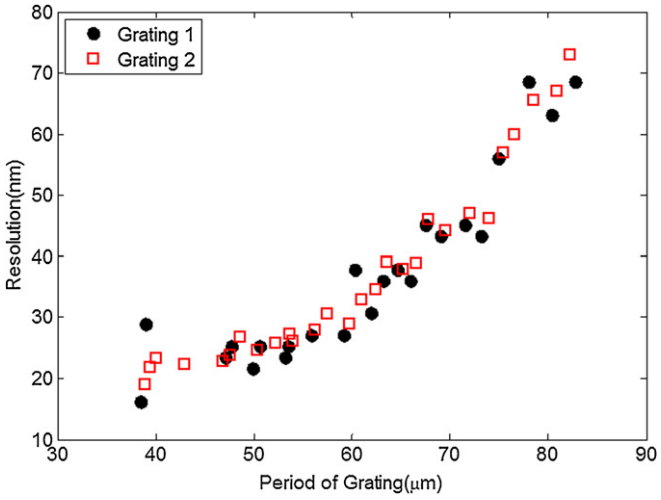

(*b*)

Figure 10. (*a*) Plot of the measured intensities along the grating to determine spectral resolution at each grating period and (*b*) spectral resolution at each period of the grating without actuation (measurement from two different gratings).

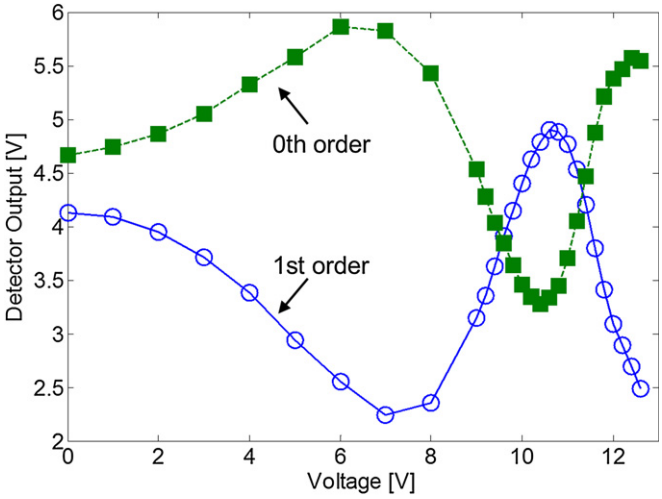

Figure 11. Detector output variations at zero and first orders while changing dc bias to the electrode.

difference in scanning. The experimental results demonstrate that the resolution is better at the fine grating due to the larger dispersion angle.

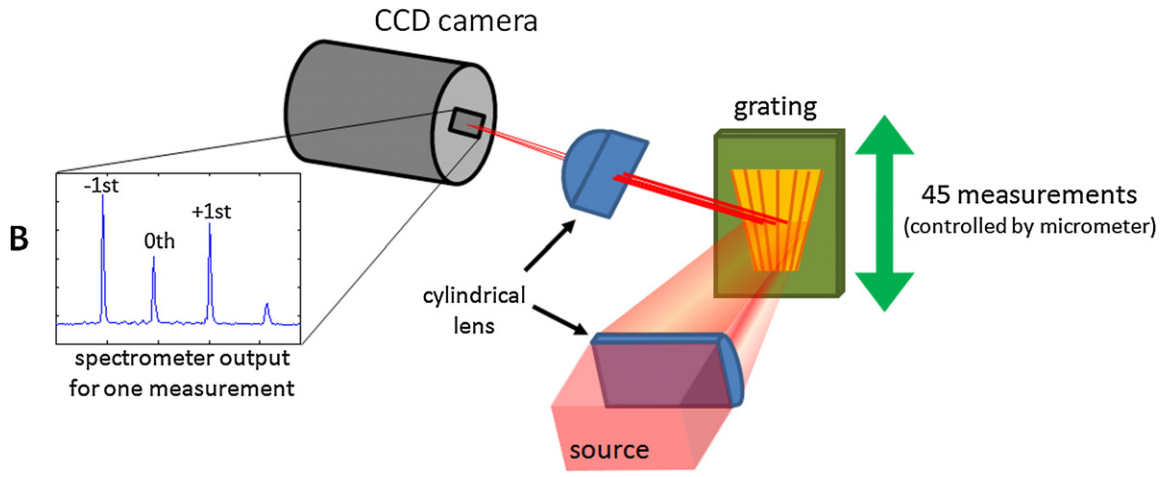

(*a*)

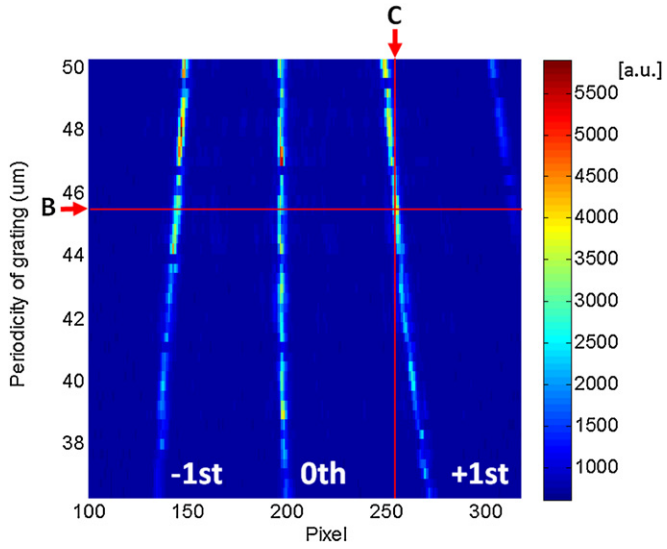

(*b*)

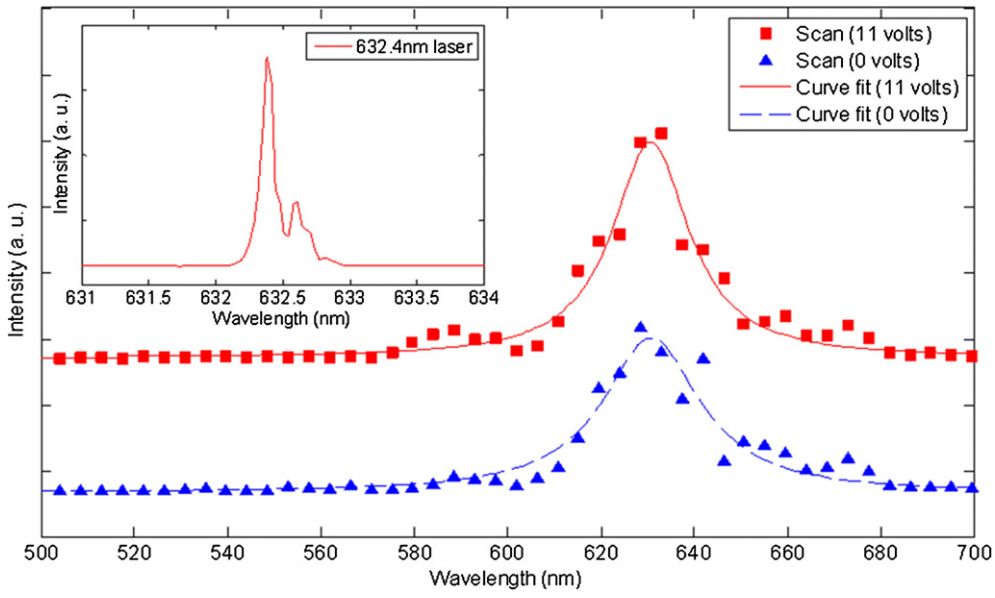

(*c*)

Figure 12. (*a*) Experimental setup to capture CCD camera intensity readings for an excitation of 0 and 11 V on the grating, (*b*) intensity from the grating for the 45 measurements shown as B depicted in (*a*), (*c*) intensity from a single detector (line C). Inset: measured resolution from a commercial spectrometer for the same HeNe laser.

To demonstrate maximization of the intensity at first order, the focused light beam is fixed at an approximately 52 μm period of the grating and the step height is adjusted by applying a dc bias between the suspended beam and the electrode underneath. Figure 11 shows the variation of photodetector output at first order as the voltage bias is increased, and the maximum is found at 10.8 V. It means that 10.8 V needs to be applied to earn the maximum intensity at the first diffraction order while detecting a 0.633 μm wavelength at the 52 μm period of grating. It appears that at 0 V, the intensity is close to another maximum. Thus, from 0–10.8 V, the grating travels around 317 nm, which is closely matched with height travel measured in figure 6(*c*) showing 340 nm travel at 11 V. Note that the actuation voltage needs to be changed at each band. In this measurement, a hybrid silicon detector with low noise transimpedance amplifier (TIA) (SD100-41-21-231, Advanced Photonix) is used. The TIA has a gain of 100 kV A^{-1}. The responsivity of the detector is 0.38 A W^{-1} at 633 nm. This experimental result can be compared to the plot shown in figure 3(*d*) where the *x*-axis is the grating height. The grating height, $d = 9.96$ μm, at 0 V is seen in the description shown in figure 6(*b*). In figure 3(*d*), it is equivalent to $d = 3\lambda/4 = 0.47$ μm by calculation of 9.96–0.633∗15 = 0.47. Therefore, the first order is close to a maximum at 0 V and another maximum at 10.8 V which is equivalent to $d = \lambda/4$ as shown in figure 3(*d*).

Ideally the lowest intensity at each order is zero if the reflection coefficients of the top and bottom surfaces are the same as seen in the analysis. However, the reflection from the bottom layer is weaker (measured reflection coefficient of 0.239) than that from the gold top layer (measured reflection coefficient of 0.782), producing a non-zero intensity at the minimum. The reflection coefficient of the surface is measured optically using a photometer and a HeNe laser. The reflection coefficient of the bottom layer is estimated from a rectangular gold–silicon substrate pattern shown in figure 4(*a*) and the reflection coefficient of the bottom layer is measured from the bond pad shown in figure 4(*a*) since they are fabricated under the same conditions as the bottom and top layers, respectively. From figure 5(*b*), it is found that the bottom surface is much rougher than the top surface, making the bottom a less reflective surface. This may contribute to the low reflectivity from the bottom layer.

To demonstrate its operation as shown in figure 1, the grating is tested using another CCD camera (Princeton Instruments ACTON PIXIS 400), selecting only one pixel on the camera to act as a detector. The experimental setup is the same as shown in figure 9 except for the camera. The CCD camera, used in commercial spectroscopy (Princeton Instruments ACTON SP2150), has a large screen and a pixel size of 20 μm × 20 μm. In this experiment, spectral resolution is compared with and without the actuation voltage. Figure 12(*a*) shows the spectrometer readings of the grating over a span of 2.25 mm (36–50.4 μm period of grating) covered by 45 measurements starting from the tapered end of the grating. 11 V is applied on the grating to make the first diffraction intensity be a maximum value. 11 V is a little bit off from 10.8 V, but 11 V shows a higher intensity than 10.8 V experimentally. This experiment uses a CCD camera, acting as an array of detectors, to get multiple 'B' lines. If a single photodetector was used in the experiment, that method would be similar to selecting a single pixel location from the 'B' lines. After the controlled 45 measurements as the period of the grating is changed, a single detector would resemble the line 'C' in figure 12(*b*). The 'C' line is the spectrum of incident light collected and shown in figure 12(*c*). The resolution which is −3 dB from the peak is compared with and without voltage actuation. The inserted figure in figure 12(*c*) includes a spectrograph of the used laser peak at 632.4 nm using commercial spectroscopy. The peak's center measured from figure 12(*b*) is fixed at the 632.4 nm value. This means that a 45.6 μm grating period measures 632.4 nm. Thus, a 36 μm period measures 499 nm and a 50.4 μm period measures 699 nm based on equation (1). A Lorentzian fit is applied only to the peak of interest in the data to examine the resolution, excluding some points at the base of the peak. Without actuation, the resolution for the spectrum is 17.6 nm and is 13.1 nm with actuation as seen in figure 12(*c*). This demonstrates the deformable grating's potential for resolution improvement in spectroscopy.

The experiment also demonstrates its drawbacks. The grating needs to be actuated to collect the source light using a single detector. To avoid the actuation, an array of detectors which picks up spectra can be used as in conventional spectroscopy. Relatively large grating periods lead to limited low resolution. The micromachining technique, PolyMUMPs in this case, can only reach a certain minimum dimension in fabrication and limits the size of the grating. Advancement of fabrication technology can enable creation of deformable fine pitch gratings.

5. Conclusion

A micromachined vertically deformable varying-pitch grating is designed and fabricated. Characterization of the grating for a spectrometer is presented. The grating is useful as a spectrometer determining the source light spectrum by measuring the intensity at first-order diffraction from a single predetermined detector. From the characterization, the deformable grating shows an actuation range of 0.7 μm at 13 V. This range is wide enough to demonstrate the advantage of the grating's ability to maximize the intensity of the first diffraction order using a dc bias between the moving grating and the fixed electrodes. Its bandwidth is measured to be 3.6 kHz. Its resolution as a spectrometer is estimated to be 17–73 nm using a HeNe laser in the assumption of its detectable range being from 0.633 to 1.477 μm. With the actuation of the grating, the grating also demonstrates the capability to improve spectrometer resolution, shown from experimentation. It also demonstrates its drawbacks such as the requirement of physical scanning for a single detector and its low resolution. By using a customized fabrication process, one can reduce the grating period further, thus increasing the diffraction angle and hence the spectral resolution.

Acknowledgments

The authors would like to thank Drs Jayant Kumar and Mengyan Shen in the Department of Physics at UMass Lowell for their spectroscopy used in this paper.

References

[1] Solgaard O, Sandejas F S A and Bloom D M 1992 Deformable grating optical modulator *Opt. Lett.* **17** 688–90
[2] Zhou G, Logeeswaran V J, Chau F S and Tay F E H 2004 Micromachined in-plane vibrating diffraction grating laser scanner *IEEE Photonics Technol. Lett.* **16** 2293–5
[3] Burns D M and Bright V M 1998 Development of microelectromechanical variable blaze gratings *Sensors Actuators* A **64** 7–15
[4] Merlo S, Annovazzi-Lodi V, Benedetti M, Carli F and Norgia M 2006 Testing of "Venetian-Blind" silicon microstructures with optical methods *J. Microelectromech. Syst.* **15** 588–96
[5] Yee G M, Maluf N I, Hing P A, Albin M and Kovacs G T A 1997 Miniature spectrometers for biochemical analysis *Sensors Actuators* A **58** 61–6
[6] Hocker G M, Youngner D, Butler M, Sinclair M, Plowman T, Deutsch E, Volpicelli A, Senturia A and Ricco A J 2000 The polychromator: a programmable MEMS diffraction grating for synthetic spectra *Proc. Solid-State Sensor and Actuator Workshop* pp 89–92
[7] Sagberg H, Lacolle M, Johansen I, Løvhaugen O, Belikov R, Solgaard O and Sudbø A S 2004 Micromechanical gratings for visible and near-infrared spectroscopy *IEEE J. Sel. Top. Quantum Electron.* **10** 604–13
[8] Manzardo O, Michaely R, Schädelin F, Noell W, Overstolz T, De Rooij N and Herzig H P 2004 Miniature lamellar grating interferometer based on silicon technology *Opt. Lett.* **29** 1437–9
[9] Kung H L, Bhalotra S R, Mansell J D, Miller D A B and Harris J S 2002 Standing-wave transform spectrometer based on integrated MEMS mirror and thin-film photodetector *IEEE J. Sel. Top. Quantum Electron.* **8** 98–105
[10] Lammel G, Schweizer S and Renaud P 2001 MEMS infrared gas spectrometer based on a porous silicon tunable filter *Proc. 14th IEEE Int. Conf. on MEMS* pp 578–81
[11] Goodman J W 1996 *Introduction to Fourier Optics* (New York: McGraw-Hill)
[12] Lizuka K 1983 *Engineering Optics* (Berlin: Springer)
[13] Kim B, Schmittdiel M, Degertekin F L and Kurfess T R 2004 Scanning grating microinterferometer for MEMS metrology *J. Manuf. Sci. Eng.* **126** 807–12
[14] Kim B, Degertekin F L and Kurfess T R 2007 A micromachined scanning grating interferometer for the out-of-plane vibration measurement of MEMS *J. Micromech. Microeng.* **17** 1888–98
[15] Carter J, Cowen A, Hardy B, Mahadevan R, Stonefield M and Wilcenski S 2005 *PolyMUMPs Design Handbook* available at http://www.memscap.com/__data/assets/pdf_file/0019/1729/PolyMUMPs-DR-13-0.pdf
[16] Bifano T, Krishnamoorthy Mali R, Dorton J, Perreault J, Vandelli N, Horenstein M and Castanon D 1997 Continuous membrane, surface micromachined, silicon deformable mirror *Opt. Eng.* **36** 1354–60